High Momentum Flow Region and Central Recirculation Zone Interaction in Swirling Flows

Marco Osvaldo Vigueras-Zuniga[1], Agustin Valera-Medina[2], Nick Syred[2], Phil Bowen[2]

[1] Facultad de Ingeniería, Universidad Veracruzana, Veracruz, México.

[2] Gas Turbine Research Centre, Cardiff University, Wales, United Kingdom.

Abstract

'Fuel-flexible' gas turbines will be required over the next 20 years at least. However, this contrasts with recent experiences of global operators who report increasing emissions and difficult combustion dynamics with even moderate variations in the fuel supply. Swirl stabilized combustion, being the most widely spread technology to control combustion in gas turbines, will be a technology needed for dynamic stabilization of the flow field. However, the features of the recirculation zone are highly complex, three dimensional and time dependent, depending on a variety of parameters. A high momentum flow region inherent to swirling flows has attracted the attention of several groups interested in blowoff and stretch flame phenomena. Therefore, this study focuses on experimental results obtained to characterise the relation between the central recirculation zone and the high momentum flow region under moderate swirl levels using a well-studied tangential swirl burner for power generation applications. As to be expected the recirculation zone and the high momentum flow region rotate together about the central axis. Moreover, the interaction between them produces high, intense local velocities. This region of High Momentum (shearing flow) also presents a complex geometry that seems to be based on the geometrical features of the burner, different to previous findings on the burner where the system was thought to have a unique shearing flow region. The high three dimensional

interaction of these structure is confirmed at the point where the precessing vortex core losses its strength.

Keywords: Swirling Flows; Central Recirculation Zone (CRZ); High Momentum Flow Region (HMFR).

Nomenclatura

A_e	Tangential inlet Area [m^2]
CRZ	Central Recirculation Zone
CoRZ	Corner Recirculation Zones
D	Exit diameter of burner
$\partial U/\partial x$	Gradient of U with respect to x, [1/s]
$\partial U/\partial y$	Gradient of U with respect to y, [1/s]
G_x	Axial flux of axial momentum, [kg m^2/s^2]
G_θ	Axial flux of radial momentum, [kg m^2/s^2]
HMFR	High Momentum Flow Region
PVC	Precessing Vortex Core
r	Radius, [m]
r/D	Normalized radial position, [-]
S	Geometrical Swirl Number [2]
U	Axial velocity component, [m/s]
V	Radial velocity component, [m/s]
U/W_{inlet}	Normalized axial velocity, [-]
W	Tangential velocity, [m]
W_{inlet}	Tangential inlet velocity, [m]

x/D	Normalized length beyond burner exit, [-]
φ	Overall Equivalence Ratio [-]
σ	Standard deviation [m/s]

1. Introduction

Clearly there are significant challenges for fuel flexible gas turbines, particularly emission control and combustor dynamics, and this may well reveal considerably more complexities for the designer. As increasing fuel flexibility is required, the use of new fuels will produce a significant change in flame dynamics [1-2]. A change in flame behaviour can result in either blowoff or flashback which can have dramatic consequences to consistent low emission operation and structural integrity. Although it is very rare to find stable flames in theory, in reality these often have self-stabilizing mechanisms. In swirling flows, the crucial feature is the formation of a central recirculation zone (CRZ) which extends blowoff limits by recycling heat and active chemical species to the root of the flame in the burner exit [3-4]. Thus, the CRZ is one of the mechanisms for flame stabilization that through an aerodynamically decelerated region creates a point where the local flame speed and flow velocity match [5], whilst also providing a well stirred reactor region for flame stability. Although swirling flows are widely used in power generation with stabilizing CRZs, unless the CRZ size and shape are properly controlled, problems can arise.

Usually, a Swirl number defining the ratio of the axial flux of angular momentum to the product of the axial momentum flux and a characteristic radius is used to define the swirling features of any flow [2]. When the Swirl number reaches a critical value between 0.5 and 0.6, a vortex breakdown is observed. The pressure tends to decrease where strong swirling motion occurs in the wake of the combustor nozzle. As the flow expands and the

azimuthal velocity decays with the axial distance, the pressure is recovered. A positive pressure gradient is generated along the axial axis, leading to a recirculation zone [6].

Research groups interested in blowoff have started working on the theories behind this phenomenon. Studies that have been conducted produce a large database on how to improve operability with natural gas, but there is still plenty of work to do on the fundamental behaviour underlying combustion stability using alterative/unconventional gases [7-8]. As discussed by Shanbhogue et al. [9], there are different theories about blowoff. Longwell et al. [10] suggested that blowoff occurs when it is not possible to balance the rate of entrainment of reactants into the recirculation zone, viewed as a well stirred reactor, and the rate of burning of these gases. Since entrainment rates scale as the size of the CRZ increases and velocity of the flow is decreased, then it follows that this criterion reduces to a Damköhler (Da) number blowoff criterion, using a chemical time that is derived from the well stirred reactor [9]. A similar idea relates to blowoff occurring when the heat required by the combustible stream exceeds that received from the recirculation zone. This leads to the same entrainment based, fluid mechanical time scaling as above.

A different view is that the contact time between the combustible mixture and hot gases in the shear layer must exceed a chemical ignition time. This leads to scaling the characteristic dimension by the recirculation zone length, leading to a similar Da criterion. As such, blowoff theories postulating the existence of well-stirred reactor regimes, such as in the recirculation zone, seem to capture most of the controlling features of the processes, although there are differing views [9].

Some blowoff theories are based on a flamelet based description via local extinction by excessive flame stretch [11]. Flame stretching starts blowoff with the initiation of holes in the flame, that are healed by the same flame creating stretching in areas that otherwise

would have been unaffected. The flame will extinguish when flame stretch rate exceeds a critical value [5]. However, it is also recognized that this mechanism is not the one causing the final blowoff, as it is clear from data that the flame can withstand some extinction [12-13]. Therefore, it is considered that the "critical extinction level" is somehow influenced by other mechanisms [9].

Regarding the central recirculation zone, the use of different configurations has demonstrated that the shape and strength of the CRZ can change drastically depending on these alterations. Researchers [4, 14] have observed how the change of the combustor nozzle can produce different central recirculation zones under the same injection conditions. The use of a 0.8D square nozzle produces a larger structure, whilst a quarl nozzle creates a more compact, stronger CRZ. A normalized CRZ velocity was calculated from PIV measurements and it was observed that the quarl produced a negative velocity ~80% stronger than the one observed using the square nozzle. This velocity increment was accompanied by a reduction in size of ~11%, as the CRZ was compressed by pressure gradient changes as a consequence of the sudden expansion at the nozzle exit. However, it was clear that the width of both structures was almost the same, as most of the shear flow leaving the nozzle was of similar high axial velocity.

A rotating time dependant high momentum flow region (HMFR) associated with the CRZ and swirling flows has also been document by several authors [2, 14-15]. The CRZ is displaced from the central axis, precesses about it and generates the asymmetric High Momentum Flow Region (HMFR) located in the shear layer. This phenomenon is often accompanied by a Precessing Vortex Core (PVC). The generation mechanisms for these events is unclear. Some authors have studied the phenomena under isothermal conditions [16-17] producing concepts involving the movement of these coherent structures as a

manifestation of the compressing-expansive mechanism in the inner part of the structure, whilst others have theorised its nature as a series of small eddies generated by the CRZ [6]. Paschereit and Gutmark [18] have proposed that small Kelvin-Helmholtz vortices are produced by the difference in momentum and density of the flows. These small vortices find a common path energized by the CRZ, whose exchange of momentum allows the development of larger structures such as the PVC, which starts precessing around the system. The highly complex nature of these structures has been studied by some [19-20] but there is still considerable room for research on how these structures affect the combustion stability limits. Yazdabadi and Syred et al. [21-22] showed that despite the considerable asymmetry of the exhaust flow using swirling flows, the angular momentum of the flow is equal on both sides of the rig, taking as reference point the centre of the PVC. Thus, the angular momentum is conserved by being squeezed through the region of the HMFR. The faster the PVC/CRZ, the narrower the area gets. Therefore, it seems logical that the interaction between these structures is very important, especially for the study of blowoff mechanisms.

2. Setup

Experiments were performed in a 100kW steel scaled version of a 2MW swirl combustor [4]. Two tangential inlets were used together with blockages of 25% of the width of the tangential inlet to provide a swirl number of 0.98. The system was fed by a centrifugal fan providing air flow via flexible hoses and two banks of rotameters for flow rate control and a further bank for natural gas injection. The burner geometry is depicted in figure 1. A diffusive injector was utilized to provide partially premixed conditions. The burner was operated using natural gas, with 25 l/min diffusive -40 l/min premixed injection. 1600 l/min of air were injected, giving an overall equivalence ratio of φ=0.386, close to blowoff. A

quartz, open ended cylinder was used to visualize the flame being attached to the burner exit by appropriate fixing lugs and flanges. A burner exhaust confinement with conical contraction of 45° angle was added, with an aperture of 1.0D, figure 2. Access to the inner system was performed using a cylindrical cylinder quartz of 130 mm. The area expansion ratio for this combustor is 3.61. This geometry is representative of industrial combustors. Due to reflection caused by the cylindrical shape of the quartz, masks were placed in front of the CCD camera in order to avoid saturation and damage to the CCD sensors. This reflection only occurred near the walls, therefore restricting measurements only in this area. The posterior wall was painted with a black, high temperature resistant paint, to reduce signal noise.

The HMFR and associated regular pressure signal allowed the triggering of a velocity measurement system, providing space resolved results. Pressure fluctuation measurements were made with an EM-1 Yoga Electret Condenser Microphone, with a frequency response of 20 Hz-16 kHz and sensitivity of -64±3 dB. It was positioned 30mm upstream from the burner exit [14, 23] as used by others [24].

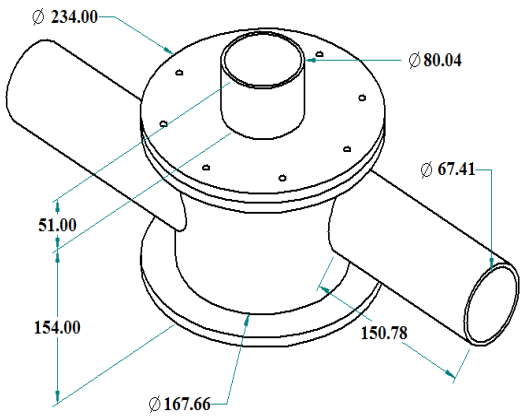

Figure 1. Burner geometry [mm]. D = 80.04mm.

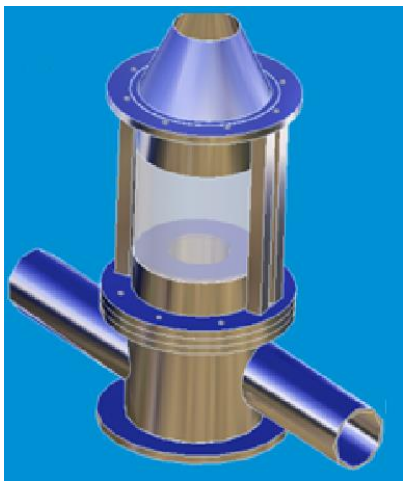

Figure 2. Conical swirl exhaust.

This microphone condenser signal was redirected to a signal conditioner with low and high band pass, allowing the recognition of smoother signals. These were redirected to trigger a BNC Model 500 Pulse Generator, whose TTL signal was sent to a Dantec PIV system. The latter consists of a dual cavity Nd: YAG Litron Laser of 532 nm capable of operating at 5 Hz, a Dantec Dynamics laser sheet optics (9080X0651) was used to convert the laser beam into a 1 mm thick sheet. To record the images a Hi Sense MkII Camera model C8484-52-05CP was used, with 1.3 MPixel resolution at 8 bits. A 60mm Nikon lens was used for resolution purposes with a field of view of approximately 750x750 mm, with a resolution of 2.31 pixels per mm and a depth of focus of 5.8 mm. The inlet air was seeded with aluminum oxide Al2O3 by a venturi system. The entire system was triggered at 90% of the highest peak observed after 5 minutes of free running, as in previous studies [2, 4].

Experiments were conducted to recognise the highly three dimensional shape and interaction of the CRZ and the HMFR. Due to the precession of the CRZ-HMFR and the planar nature of the axial radial velocity planes, measurements were obtained by moving the Laser circumferentially around the outlet lip sequentially by 11.25° (32 planes in 360°) to allow a complete study of both structures. Each phase plane will be referenced according to the position where the Laser was placed during their acquisition.

The CRZ was characterized via the position of near zero axial velocities. The HMFR was obtained using a criteria of 90%, 50% and 30% of the highest velocity in order to define a good correlation between planes. A tomographic reconstruction at 4.9 m/s (50% of the highest, coherent velocity measured in the U velocity map) was performed. Although this value is arbitrary, the tomographic reconstruction of the system using these values provided coherent results as presented latter. After acquisition of the PIV data, a frame-to-frame adaptive correlation technique was then carried out with a minimum interrogation area of

32x32 pixels and a maximum of 64x64, with an adaptivity to particle density and velocity gradients. A mask was used on the frames to focus on an area of 130x150mm. 75 pairs of frames per plane were used to create an average phase locked velocity map after tests showed 150 pair of frames gave similar results in an independency test campaign. This analysis was later extended to study different velocity levels in the CRZ and the HMFR. A vector substitution was performed, with only 2.8% of vectors removed, giving high confidence on the remaining vectors. The high accuracy of the results is deemed to the careful focusing of the image, correct injection of particles, masking of regions with very low flow and software correction based on particle density and velocity gradients. The velocity maps for the field were developed over the range of -2.2 to 8.8m/s for U, -6.7 to 5.1m/s for V, and 0.0 to 9.8m/s for total velocity, where ~97% of the velocity vectors appeared. A velocity variance analysis was also performed on the boundaries of the CRZ and the HMFR giving values between 0.0 and up to 13.1m^2/s^2, depending on their position. The frequency of the CRZ was observed to be around 100Hz for this configuration. This is in accord with other studies [2, 4]. In order to reduce the parallax error, the line of view of the camera was positioned exactly in the middle of the nozzle using a physical grid provided by the laser manufacturer. The field of view was calibrated until having the central line of the burner in the centre of the grid, thus ensuring that the position of the system would not affect the results.

3. Results and Discussions

Several planes were obtained from this work to produce a tomographic reconstruction of the interaction between the CRZ and the HMFR. The high accuracy of the results and the correlation techniques, Figure 3, would allow the link between planes, thus providing

details of the coherent structures, Figure 4. It can be observed how the planes evolve. In order to assess the distribution of results, a variance analysis was performed, Figure 5.

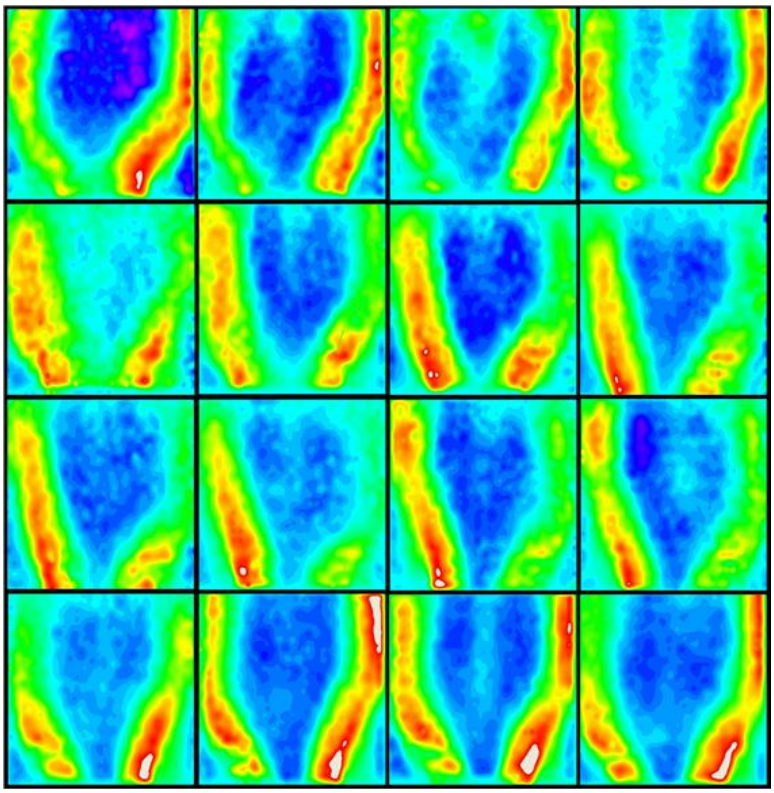

Figure 3. Velocity map progression between planes. It is clear how the HMFR (red region) in the first plane converges with the one in the last plane.

It can be observed that the regions that correspond to the CRZ, the corner recirculation zones (CoRZ) and the developed HMFR show the lowest values between 0.0 and 2.8m^2/s^2. Parts of the HMFR closest to the CRZ, showed highest variance, with its greatest value being located at the positions where the HMFR shows its fastest, positive velocities (now on, referred as Triggering HMFR). Nevertheless, it is on the right hand side of the profile that the variance reaches its highest peak at 13.1m^2/s^2. Therefore, the distribution of results in this region is widely spread, as this is the point of interaction between the CRZ and the HMFR.

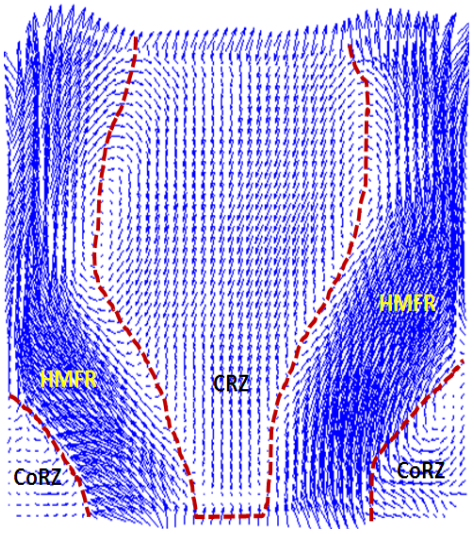

Figure 4. Velocity vector map. CRZ and CoRZ show negative values. HMFR denotes positive velocities. Plane 0-180°.

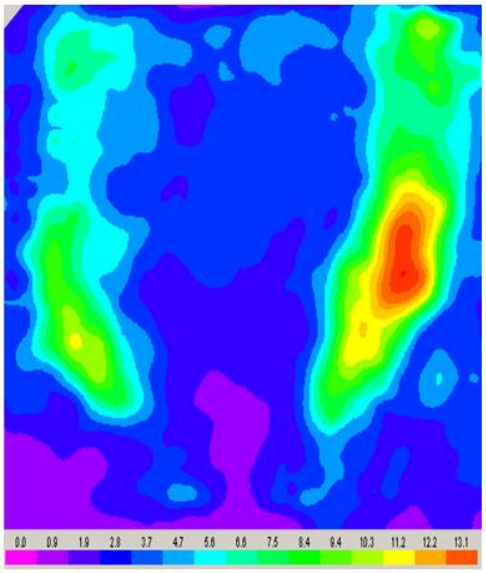

Figure 5. Variance analysis, 150 frames. Plane 0-180°.

Total velocity maps, Figure 6, were analysed to observe the strength of the HMFR and CRZ. The flow profile is producing a very strong central recirculation zone, which is pushed by the HMFR on both sides. The HMFR velocity intensity on both sides seems to be similar, in a range between 7.0 and 9.8m/s, although the Triggering HMFR on the right is more elongated. However, the position of highest velocity on both sides is at similar

distance downstream the nozzle (bottom limit of the PIV frames). Therefore, a further decomposition of the velocity field was required. Velocity maps for the V and U components were obtained, Figures 7 and 8.

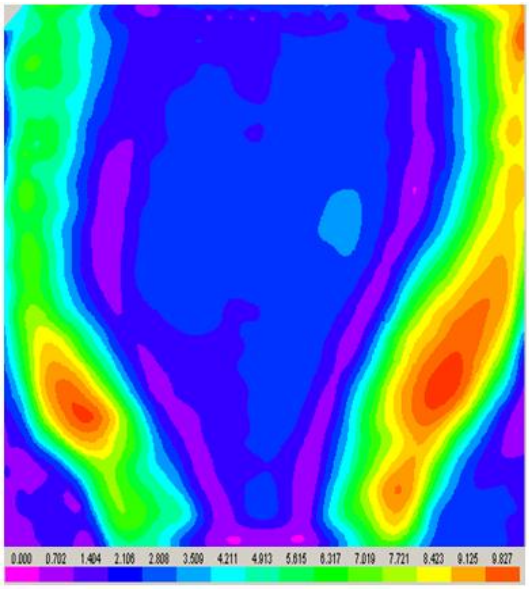

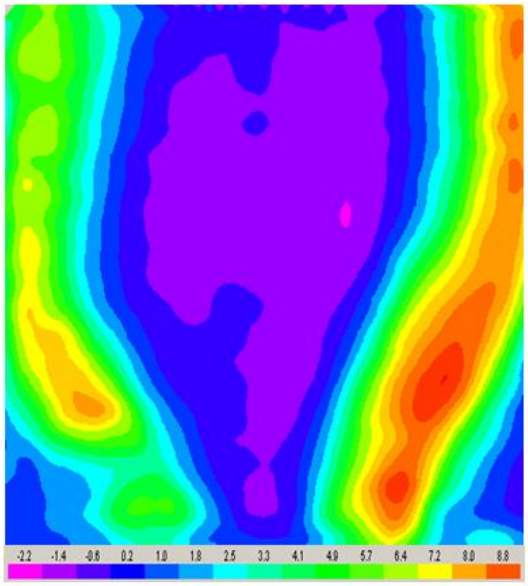

Figure 6. Total velocity map, plane 0-180°. **Figure 7**. Axial velocity, U, plane 0-180°.

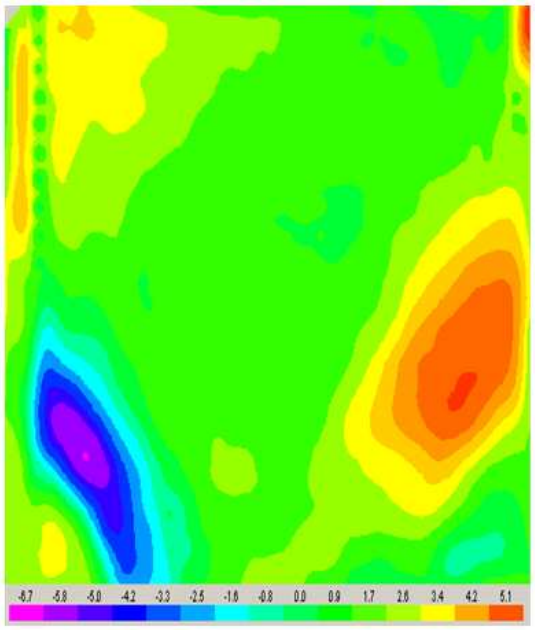

Figure 8. Radial velocity, V, plane 0-180°.

Figure 7 shows how the axial component U is stronger with the Triggering HMFR. Moreover, the CRZ shows its most negative peak -2.2m/s just above this region of high intensity. Although the left hand side of the HMFR shows a strong velocity profile, its momentum on the right hand side overwhelms the latter. When analysing the radial V velocity component, Figure 8, although the sign relates to the position of the HMFR, absolute intensities can be compared. It is clear that the Triggering HMFR has decayed when reaching the opposite, left hand side. The radial velocity on the right is at 5.1m/s, increasing its value on the left to 6.7m/s, an increment of ~30%. Therefore, the high momentum of the HMFR on left hand side, Figure 6, is maintained by this increase in radial velocity.

Thus, the exchange of kinetic energy between the HMFR and CRZ, other coherent structures, pressure decay and the turbulence in the shearing flow between structures has altered the final momentum of the HMFR. The axial velocity of the body has been reduced whilst increasing the radial velocity as a result of the trade-off of energy between the CRZ and HMFR. As observed by others [4, 21] the axial flux of angular momentum, G_θ, which is related to the tangential velocity and the Swirl number, changes locally as well. The local angular momentum is reduced in the region opposite to the Triggering HMFR, leaving the local swirl of the flow at just half of the one observed in the latter [21]. Therefore, the increase of local radial momentum in the HMFR can be correlated to this local decay of axial and tangential momentum.

In terms of turbulence, O'Doherty et al. [25] showed that a great variety of eddies appeared in the vicinity of the shearing region between the CRZ and the HMFR. Although the findings were isothermal, these eddies could be responsible for a better mixing in the

vicinity of the recirculation zone, improving the burning process under combustion conditions.

Due to the lack of results in the Kolmogorov's scale, the study focused on the exchange of energy between the axial and radial components. This was studied through the analysis of $\partial U/\partial x$ and $\partial U/\partial y$ gradients, as the derivatives of V did not gave useful results due to their low relative values. Figure 9 shows how $\partial U/\partial y$ increases on the right hand side where the interaction between the CRZ and HMFR is just happening, with the highest values observed at ~0.5-0.6D from the nozzle. High gradients are observed within the CoRZ. On the other hand, the left hand side profile shows some variation in $\partial U/\partial y$, still this is just half of the observed on the right hand side. Figure 10 shows how $\partial U/\partial x$ is minimal when compared to $\partial U/\partial y$. Thus, the value of U is varying considerably on the radial direction. This implies that the stabilization process of the CRZ is modifying the axial velocity of the HMFR through the increase of its radial component, making the HMFR to rotate while exchanging axial kinetic energy with the CRZ. Thus, the remaining HMFR, on the left side, will have a higher radial flux of momentum.

The position of high gradient at ~0.6D can be also correlated to previous studies. Valera-Medina et al [17] showed that the position where the Precessing Vortex Core (PVC) losses its helical nature is around this region. Probably, the high interaction between the CRZ and HMFR at this position, combined with the interaction of the PVC, reduce the energy of the last 2 whilst increasing the intensity of the CRZ. The PVC would become weaker, with more axial energy exchange in this region, making its helical shape very erratic. Nevertheless, this is a point that requires further studies.

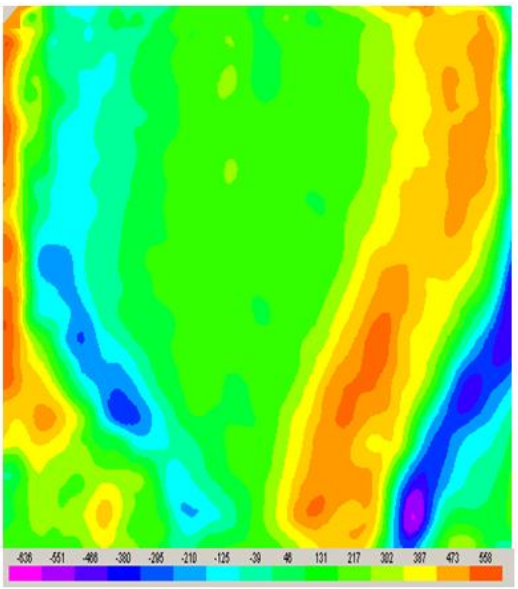

Figure 9. ∂U/∂y, plane 0-180°.

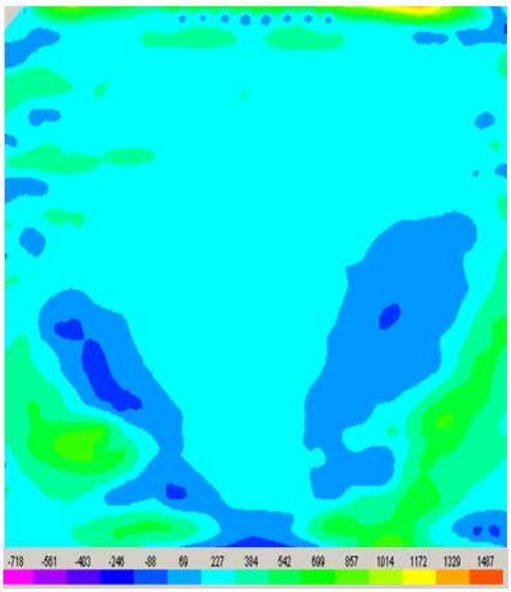

Figure 10. ∂U/∂x, plane 0-180°.

The energy exchange between the CRZ and HMFR can be also observed in the velocity profiles across the entire field, Figures 11 and 12. Radial velocities were obtained at different axial positions, Figure 11. A normalization of the axial velocity was done using the tangential inlet velocity, W_{inlet}, equal to 3.74m/s for this configuration. The results show that the most negative region is located between 1.0D and 1.2D from the nozzle, whilst the most positive peak can be found at 0.6D from the nozzle. The negative vectors are confined inside of the CRZ, with the strongest values far away from the centreline and close to the region of interaction with the HMFR. A similar analysis was performed, but obtaining the axial velocity profiles at different radial positions, Figure 12. The profile close to the centreline at -0.16r/D shows an entirely developed recirculation zone. The biggest gradients are located at 0.73r/D and 0.40r/D. The first of the latter shows a CoRZ that then is followed by the HMFR. The second one at 0.40r/D denotes a very strong HMFR followed by a very strong CRZ that is more intense than the structures formed at -0.49r/D from the centreline, on the left hand side. Therefore, this confirms the previous assertions.

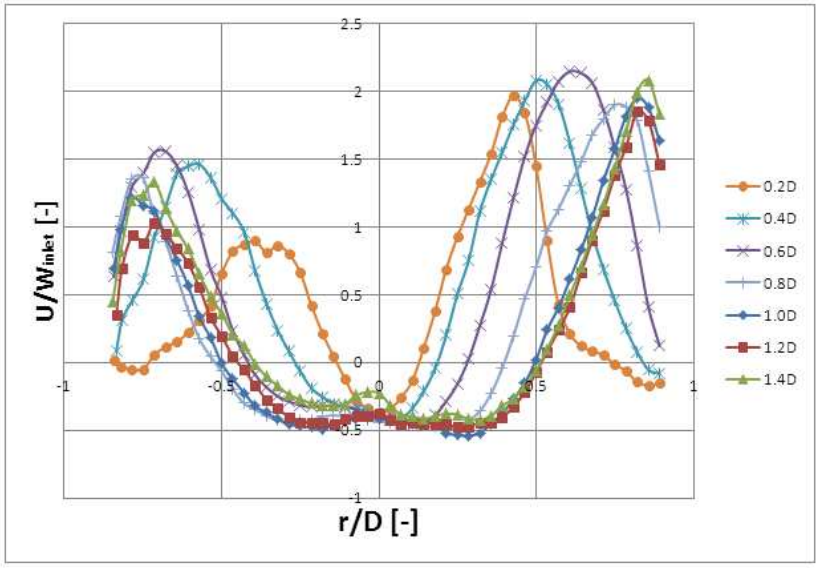

Figure 11. Axial velocities at different axial positions, plane 0-180°.

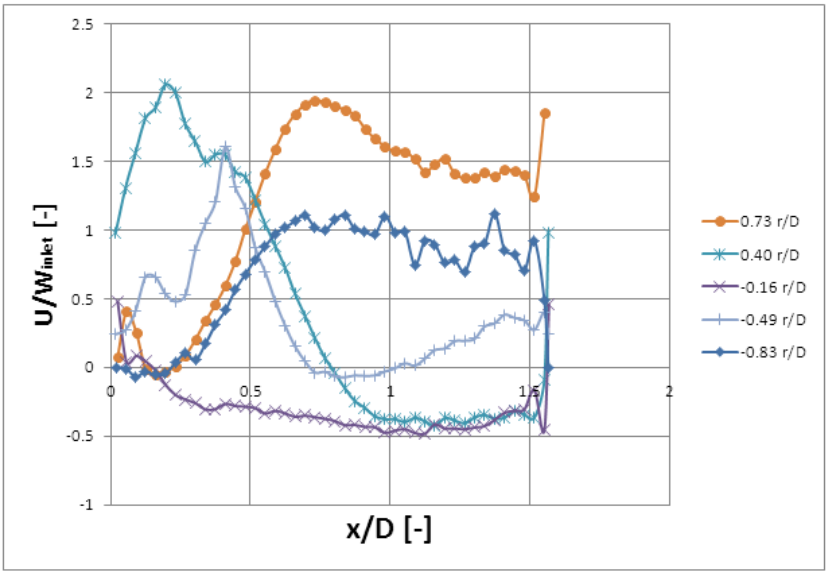

Figure 12. Axial velocities at different radial positions, plane 0-180°.

A dimensionless analysis of the ratio of the axial and radial velocities for all the planes was performed. The velocities ranging from 0.98 to 9.8m/s (90%), 4.9 to 9.8m/s (50%) and 6.8 to 9.8m/s (30%) were used in order to find the correlation between planes. A 2σ, 95% statistical analysis was applied to all the data, giving more confidence of the results by eliminating those points where the ratio was too high and out of range. Interesting results

were observed, Figure 13. The 30% case did not give enough data for a statistical analysis, thus was not included. The 90% and 50% analysis provided good information about the flow. Results show averages for all planes as a function of phase angle.

The 90% case shows a flow that presents 3 high peaks of axial velocity. The highest peak appears in the range of 225-240°. This would be a problem, as the system was triggered by the first peak located at 0-45°. Thus, a closer analysis recognised that the highest ratios were produced by those vectors located in the inner and outer shear layers of the flow [19] with extremely low radial velocities. Eliminating these regions through the 50% analysis, a region of high axial velocity in the range of 0 to 45° was observed. As discussed, this is the triggering HMFR. The axial values suddenly decay, as part of the energy is transferred to the surrounding CRZ. However, the second high peak HMFR in the range of 225 and 250° still appears in the analysis. This region was expected to have a very low axial velocity, although it gives some insights of high axial velocity versus the radial component. The only explanation that has been found is the one related to the geometry of the burner, Figure 14. The air inlets are located at angles of ~45° and 225°, thus some extra velocity comes from the second inlet to increase the energy of the HMFR in this side of the burner. It is notable that the triggering occurs at very high HMFR velocities, thus most of the air is being compressed by the CRZ and conjoined structures. However, the HMFR evolves following a trend similar to the PVC. The system is creating a structure, the HMFR, that moves based on the geometrical patterns of the incoming air. If this is the case, then the structure must have developed its geometrical patterns from the beginning of the experiments, keeping the latter even after a long period of time. Its interaction with other structures and the geometry of the burner have influenced little on the final profile of the structure. Thus, the HMFR

could be traced from the point when it was created, based on the shape and characteristics of the incoming flow.

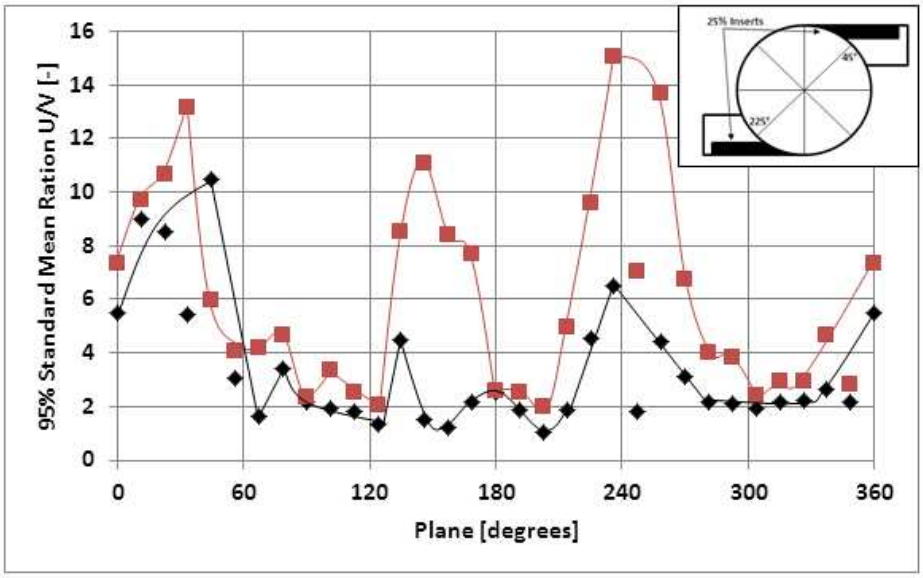

Figure 13. Mean ratio U/V for all the planes.

A third peak in the range of 120-180° appears in both cases, Figure 13. As the inner and outer shear layers are kept, i.e. 90% case, the peaks are very high. However, when these are removed, i.e. 50% case, the peak left is very small. Thus, the inner and outer shear layers become stronger in the region located between the HMFRs. The only strong structure in this vicinity is the CRZ. Therefore, although the CRZ is moving with the HMFR, the high strength of the former is kept along its entire surface, peaking in both locations where it gets in contact with the HMFR in order to sustain itself and in places where no HMFR is present thus having space to propagate. As presented by O'Doherty and Gardner [25], the CRZ is providing energy to the flow to increase its axial velocity in this region probably via the creation of strong eddies inside of the CRZ that move towards the regions where the body can propagate due to the lack of a forcing flow such as the HMFR.

A decomposition of the U/V ratios was done in 3 parts, i.e. 0.0-0.6D, 0.6-1.2D and 1.2-1.8D, for each plane, Figure 14. The first region, close to the nozzle and squeezed by the CRZ and the corner recirculation zones seems very stable, with only a considerable peak between planes 0° and 45°. The intermediate region where the flow starts to lose its radial velocity located between 0.6 and 1.2D is more unstable, with high peaks in the planes between 120-180° and 225-270°. Finally, the outgoing flow with a very low radial component shows high ratios between its axial and radial velocities in the first planes, planes located between 120° and 180° and finally the rest of the flow beyond 225°. A close examination of the planes was done and it was observed that the first region remains more stable due to the high radial values produced by the first expansion of the flow and CRZ that acts as a solid body. The second region that has already suffered the expansion starts to lose its radial component and coherence. It is clear that the region most affected is the one where the CRZ has freely expanded, opposite to the triggering HMFR. Moreover, the second part of the HMFR, located between 225 and 250°, is also reducing its radial component. Although this part of the HMFR was not detected in the first zone decomposition, in the same manner as has not been observed by others [2, 21. 23], it appears downstream between 0.6 and 1.2D. Thus, it could be the remnant of the Triggering HMFR that has reached this point, or it could also be linked to the interaction with the PVC as observed by Valera-Medina et al [17], as the PVC losses its helical nature above 0.6D and gets attached primarily in just one region, i.e. from plane 225° to plane 270°. Finally, the rest of the flow, that has transmitted most of its radial energy towards the CRZ, has now a very low radial component, leaving the flow almost entirely with an axial component.

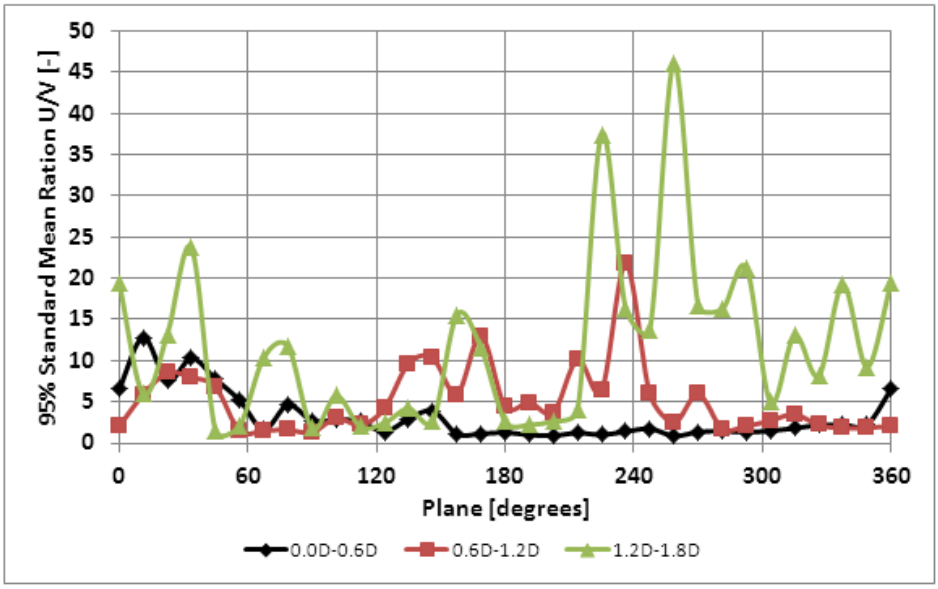

Figure 14. Zone decomposition of the U/V ratio for all planes.

In order to show how the CRZ and the HMFR travel together, a tomographic reconstruction was performed, Figure 15. A criterion of 50% velocities was used, as this provided better correlation for the HMFR, as discussed before. It can be observed that the HMFR shows the highest momentum where the CRZ is more convoluted. Although the triggering of the system is being done by the HMFR and this deforms the CRZ close the nozzle, its fast decay and the strong interaction produce a very strong CRZ downstream at a position ~1.0D. A second peak, the one located at 225-250° can also be observed.

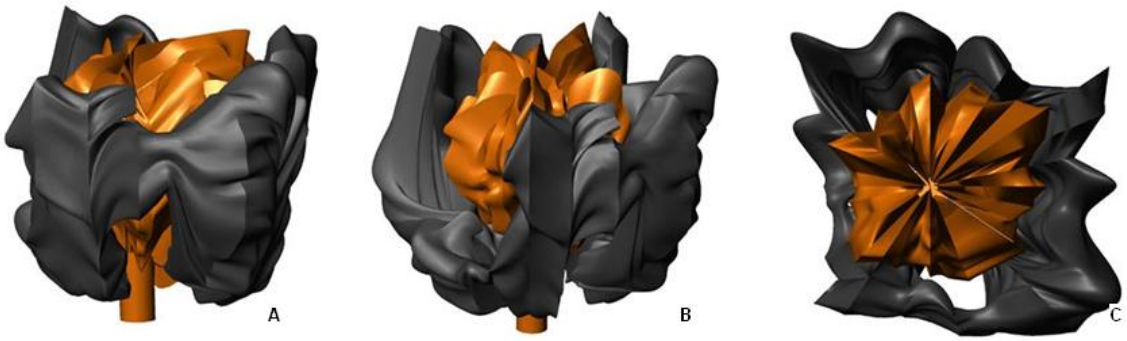

Figure 15. CRZ-HMFR interaction. Tomographic reconstruction. A) 270° rotation; B) 225° rotation; C) Top view.

This study demonstrates the complex tridimensionality of the flow field using this tangential swirl burner, with insights of the interaction between the HMFR and the CRZ. These patterns can be used to work on some theories behind blowoff. It has been observed that the HMFR will increase locally the strength of the CRZ, thus increasing the shearing stress between structures. However, this will also increase the mass flow rate of fresh reactants through the boundaries of the recirculation zone. On the other side of the array, the lack of HMFR could have been beneficial to the reduction of shear, but the reduced strength of the HMFR allows the CRZ to propagate some energy that increases the shear stress, a problem to the resistance of blowoff. This topic will require further research.

4. Conclusions

It has been observed that the HMFR and CRZ are complex structures that interact between each other in a tridimensional manner. The high coherence of the CRZ is achieved via the interaction with the HMFR, as the CRZ forms a region of high strength when it gets in contact with the HMFR. This region seems to be producing eddies that expand towards the other side of the structure, increasing the shear stress where there is not forcing flow. A secondary HMFR has been found and correlated to the geometry of the burner. Its position remains unchanged after several cycles. Although it has not been seen previously by other studies, this region seems strong enough to also stretch the flow in the opposite side of the main flow. If this is the case, then the HMFR is a structure formed by the geometrical array of the incoming air, thus it could be traced based on geometrical assumptions in these types of burners. This behaviour could be used to modify the structure in other burners, improving the resistance to blowoff. A zone decomposition analysis has showed that the first region of the flow suffers low decay of the radial component, as expected by the expansion of the flow. However, the secondary zone presents peaks of low radial

components in the secondary HMFR that could be correlated to the remnant of the triggering HMFR or the interaction with the PVC. The third zone decomposition shows high peaks as the radial component has been reduced considerably in the HMFR, with a flow that is almost entirely axial. This highly complex nature of the CRZ/HMFR/PVC contributes to the blowoff phenomenon, with shear layers that evolve with the structures of the flow.

5. Acknowledgements

The authors gratefully acknowledge the support of the Welsh Assembly Government Low Carbon Research Initiative Programme, EPSRC (grant no EP/G060053) and the European Union via various grants. Dr. Vigueras-Zuniga gratefully acknowledges the support of the Universidad Veracruzana for his visit to Cardiff University to complete this work.

6. References

[1] B. Dam, N. Love, A. Choudhuri, Flashback Propensity of Syngas Fuels, Fuel 90 (2011) 611-625.

[2] N. Syred N, A Review of Oscillation Mechanisms and the role of the Precessing Vortex Core (PVC) in Swirl Combustion Systems, Progress in Energy and Combustion Systems 32 (2) (2006) 93-161.

[3] A. Lefebre, D.R. Ballal, Gas Turbine Combustion, 3rd Edition, Taylor and Francis Group, U.S.A., 2010.

[4] A. Valera-Medina, N. Syred, P. Bowen, Central Recirculation Zone Analysis using a Confined Swirl Burner for Terrestrial Energy, J AIAA Propulsion and Power 29 (1) (2013) 195-204.

[5] T. Lieuwen, Unsteady Combustor Physics, Cambridge Press, U.S.A., 2012.

[6] T. Lieuwen, V. Yang, Combustion Instabilities in Gas Turbine Engines, AIAA, Progress in Astronautics and Aeronautics 210, U.S.A., 2005.

[7] S.G. Tuttle, S. Chaudhuri, S. Kotska, K.M. Koop-Vaughan, T.R. Jensen, B.M. Cetegen, M.W. Renfro, Time-resolved blowoff transition measurements for two-dimensional bluff body-stabilized flames in vitiated flow, Combustion and Flame 159 (1) (2012) 291-305.

[8] M. Abdulsada, N. Syred, P. Bowen, T. O'Doherty, A. Griffiths, R. Marsh, A. Crayford, Effect of exhaust confinement and fuel type upon the blowoff limit and fuel switching ability of swirl combustors, Applied Thermal Energy 48 (2012) 426-435.

[9] S.J. Shanbhogue, S. Husain, T. Lieuwen, Lean blowoff of bluff body stabilized flames: Scaling and dynamics, Progress in Energy and Combust Science 35 (1) (2009) 98-120.

[10] J.P. Longwell, J.E. Chenevey, W.W. Clark, E.E. Frost, Flame stabilization by baffles in a high velocity gas stream, Symposium on Combustion and Flame, Explosion Phenomena 3 (1) (1949) 40-44.

[11] J. Driscoll, Turbulent premixed combustion: flamelet structure and its effect on turbulent burning velocities, Progress in Energy and Combustion Science 34 (1) (2008) 91-134.

[12] T. Poinsot, D. Veynante, Theoretical and Numerical Combustion, R.T. Edwards, U.S.A., 2005.

[13] Q. Zhang, S.J. Shanbhogue, T. Lieuwen, J. O'Connor, Strain Characteristics near the Flame Attachment Point in a Swirling Flow, Combustion Science and Technology 183 (7) (2011) 665-685.

[14] A. Valera-Medina, N. Syred, A. Griffiths, Central Recirculation Zone Analysis in an Unconfined Tangential Swirl Burner with Varying Degrees of Premixing, Experiments in Fluids 50 (6) (2010) 1611-1623.

[15] G. Bulat, P. Stopford, M. Turtell, D. Frach, E. Buchanan, M. Stöhr, Predictions of aerodynamic Frequencies in a Gas Turbine Combustor using transient CFD, ASME Turbo Expo (2009) ref. GT2009-59721.

[16] S. Alekseenko, P. Kuibin, V. Okulov, S. Shtork, Helical vortex in swirl flow, J Fluid Mechanics 382 (1999) 195-243.

[17] A. Valera-Medina, N. Syred, A. Griffiths, Visualization of Coherent Structures in a Swirl Burner under Isothermal Conditions. Combustion and Flame 159 (2009) 1723-1734.

[18] C.O. Paschereit, E. Gutmark, Control of high-frequency thermo-acoustic pulsations by distributed vortex generators, AIAA Journal 44 (3) (2006) 550-557.

[19] M. Stohr, C.M. Arndt, W. Meier, Effects of Damköhler number on Vortex Flame Interaction in Gas Turbine Model Combustor, Proceedings of the Combustion Institute 34 (2013) 3107-3115.

[20] M.O. Vigueras-Zuniga, A. Valera-Medina, N. Syred, Studies of the Precessing Vortex Core in Swirling Flows, J of Applied Research and Technology 10 (3) (2012)755-765.

[21] P. Yazdabadi, A study of the Precesssing Vortex Core in Cyclone dust separators and a method of Prevention, PhD thesis, Cardiff University, UK, 1996.

[22] N. Syred, M. Abdulsada, A. Griffiths, T. O'Doherty, P. Bowen, The effect of hydrogen containing fuel blends upon flashback in swirl burners, Applied Energy 89 (2012) 106-110.

[23] J. Dawson, V. Rodriquez-Martinez, N. Syred, T. O'Doherty, The Effect of Combustion Instability on the Structure of Recirculation Zones in Confined Swirling Flames, Combustion Science and Technology 177 (12) (2005) 2341-2371.

[24] C.O. Paschereit, E. Gutmark, The Effectiveness of Passive Control Methods, ASME Turbo Expo (2004) ref. GT2004-53587.

[25] T. O'Doherty, R. Gardner, Turbulent Length Scales in an Isothermal Swirling Flow, The 8th Symposium on Fluid Control, Measurement and Visualization, 22nd-25th August, Chengdu, China, pp. 6, 2005.